Simultaneous analysis and design optimization for seismic retrofitting of hysteretic structures with fluid viscous dampers

Nicolò Pollini (nicolo@technion.ac.il)
Technion - Israel Institute of Technology https://orcid.org/0000-0001-8504-6005

Research Article

Keywords: structural optimization, hysteretic behavior, seismic retrofitting, viscous dampers, SAND

Posted Date: November 21st, 2023

DOI: https://doi.org/10.21203/rs.3.rs-3639397/v1

Simultaneous analysis and design optimization for seismic retrofitting of hysteretic structures with fluid viscous dampers

Nicolò Pollini[a,*]

[a]*Horev Fellow, Technion - Israel Institute of Technology, Faculty of Civil and Environmental Engineering, Haifa, Israel*

Abstract

This paper presents a novel optimization approach for retrofitting hysteretic structures with fluid viscous dampers. Two design scenarios are considered: structures with hysteretic behavior retrofitted with linear and nonlinear fluid viscous dampers. The size and placement of the dampers is defined using a simultaneous analysis and design (SAND) optimization approach based on nonlinear programming. The dampers' manufacturing cost is minimized, with constraints on the inter-story drifts. The optimization variables are the damping coefficients of the dampers and the structural response over time. In the proposed SAND approach, the equations of motion are treated as equality constraints of the optimization problem and are not solved directly with time-history analyses. Special design sensitivity analysis methods are not needed to calculate the gradients of the objective and constraint functions. We propose a continuation scheme on the design-driving inter-story drift constraints to effectively solve challenging problems. A sequence of sub-problems is solved considering relaxed limiting values for the drift constraints. These values are gradually decreased, and the solution obtained in each sub-problem is used as warm-start information for the subsequent sub-problem. The procedure ends when a solution that satisfies the desired limiting value of the constraints is found. The proposed approach is evaluated with reproducible numerical examples that highlight its flexibility and effectiveness.

Keywords: structural optimization, hysteretic behavior, seismic retrofitting, viscous dampers, SAND

1. Introduction

With the end of the Cold War in the early 1990s, many previously restricted technologies became available to the general public. These technologies were in many cases highly advanced and robust thanks to several years of successful deployment and continuous development for military purposes. One such technology is represented by fluid viscous dampers (FVDs). In civil engineering, FVDs transitioned from structures designed for military defense purposes to commercial buildings and bridges subjected to transient earthquake and wind loads (Taylor, 2002). In this work, we will focus on the use of FVDs for seismic retrofitting of existing structures. This consists of designing an added damping system made of FVDs to improve the performance and safety levels of an existing structure subject to potential seismic hazards. However, the applicability of the approach proposed here is not limited to the earthquake engineering field, and it could be adopted also in the case of structures subjected to different transient loads. The use of viscous dampers in earthquake engineering applications was first validated between the years 1990 and 1993, when their benefit for wind and other types of transient excitation was also shown (Constantinou and Symans, 1992; McNamara and Taylor, 2003). During a seismic event, FVDs help reduce the deformation demand on the structure by dissipating part of the energy coming from the earthquake, thus reducing the deformation demand on the structure. FVDs are one possibility among other passive energy dissipation technologies, such as friction dampers, metallic hysteric dampers, and viscoelastic dampers, as recently reviewed in Almajhali (2023). The utilization of passive energy dissipation devices has received significant attention in both academic and practical contexts. For more detailed

*Corresponding author
Email address: nicolo@technion.ac.il (Nicolò Pollini)

information, interested readers are encouraged to refer to comprehensive textbooks on the subject (Soong and Dargush, 1997; Filiatrault and Christopoulos, 2006).

There are two primary factors that significantly impact the performance of an added damping system made of FVDs. The first factor is the size of the dampers, commonly quantified by their damping coefficient. The second factor is the arrangement or distribution of the dampers within the retrofitted structure. It is important to note that these factors not only influence the structural performance, but also the overall retrofitting cost. This cost consideration becomes particularly crucial in promoting the utilization of FVDs instead of (or along with) alternative seismic retrofitting techniques. If properly sized and placed, FVDs can significantly reduce inter-story drifts, total floor accelerations, and story shear forces (Constantinou and Symans, 1993).

This motivated the development of several approaches for optimizing the size and placement of FVDs, as reviewed by De Domenico et al. (2019). Providing a comprehensive review of all the gradient-free, and gradient-based, approaches found in the literature exceeds the scope and limitations of this paper. Nevertheless, for the sake of clarity, we will mention a few examples in the following discussion. With respect to gradient-free approaches, one of the most straightforward methods is a sequential placement algorithm, initially proposed by Zhang and Soong (1992), and later modified by Lopez Garcia and Soong (2002) with slight variations. These algorithms operate essentially as sequential search processes where, at each step, a predetermined amount of damping is introduced into the structure at the location corresponding to the index with the highest value. In Dargush and Sant (2005) genetic algorithms are used for discrete optimization of passively damped structural systems. The passive elements may include metallic plate dampers, viscous fluid dampers, and viscoelastic solid dampers. An analysis-redesign approach is proposed in Levy and Lavan (2006) for the sizing of FVDs in seismic retrofitting applications. The approach follows a fully stressed design principle based on which in every iteration the damping coefficients of the FVDs are updated based on local performance indices. When an index exceeds an allowable value, the associated damping coefficient is increased proportionally; otherwise, it is decreased. Altieri et al. (2018) discuss an approach that allows to explicitly consider the variability of the intensity and characteristics of the seismic input in designing the optimal viscous constant and velocity exponent of the dampers based on performance-based criteria.

In the literature, there are also approaches that rely on gradient-based algorithms to optimize the design of FVDs. Takewaki (2000) proposed a procedure to minimize the dynamic compliance of planar frame structures with linear behavior. The dynamic compliance is expressed in terms of the transfer function amplitudes of the inter-story drifts. Lavan and Levy (2005, 2006a,b) showed the efficiency and effectiveness of nonlinear programming algorithms, coupled with adjoint sensitivity analysis techniques, to optimize the design of FVDs for seismic retrofitting of linear and nonlinear structures. An approach for optimizing the placement and size selection of FVDs was first presented in Lavan and Amir (2014). The approach relies on material interpolation techniques and sequential linear programming and allows for the simultaneous placement and size selection of linear FVDs. The work of Lavan and Amir was further extended to allow for the minimization of a realistic retrofitting cost formulation in the case of linear (Pollini et al., 2016) and nonlinear (Pollini et al., 2017, 2018b) FVDs. A key aspect in gradient-based optimization approaches is the calculation of the analytical gradients of the functions involved. One of the most convenient ways to calculate the gradients is by means of adjoint sensitivity analysis techniques. In connection to this, the optimization and adjoint sensitivity analysis of hysteretic structures equipped with nonlinear FVDs is discussed in Pollini et al. (2018a). In general, designs obtained with optimization-based design approaches may be sensitive to potential failure scenarios that were not considered in the design phases. This is also true in the case of added viscous damping systems. In recent work by the author, a novel approach to fail-safe design optimization of FVDs was proposed for seismic retrofitting applications, (Pollini, 2020). It was shown that it is possible to develop a computationally efficient framework to design optimal fail-safe damper layouts.

Most of the literature on gradient-based approaches focuses on seismic retrofitting applications, where the design of the retrofitted structure is fixed. Recently, Idels and Lavan (2021a) proposed an optimization-based approach for the simultaneous seismic design of inelastic moment resisting frames and added nonlinear FVDs. Discrete material optimization functions are utilized to achieve a desired practical oriented design for both the cross-sections of the structural elements and the FVDs' sizes, while retaining a continuous problem formulation suitable for gradient-based optimization. The seismic retrofitting of steel moment resisting frames is further discussed in Idels and Lavan (2021b). Fluid viscous dampers and negative stiffness devices are sizes and placed with an algorithm based on sequential linear programming. The retrofitting cost is minimized, while the expected loss is constrained to a predefined value.

Both gradient-free and gradient-based optimization approaches typically have an iterative nature. In every de-

sign iteration, the performance of the retrofitted structural system is evaluated with expensive time-history analyses by integrating numerically the equations of motion in time. These approaches are classified as nested analysis and design (NAND) optimization approaches (Christensen and Klarbring, 2008). In what follows, we propose a novel approach for seismic retrofitting of nonlinear hysteretic structures that does not require the repeated solution of expensive time-history analyses. We consider two design scenarios that involve retrofitting hysteretic structures using linear and nonlinear FVDs. The design variables for the FVDs are their damping coefficients. In the case of nonlinear FVDs, the design extends indirectly also to the stiffness of their supporting braces. The objective is to minimize the manufacturing cost of the FVDs while ensuring that the inter-story drifts do not exceed specified limits. The response of the structural system and the size and placement of the FVDs are optimized simultaneously within a unified formulation. Structural response quantities, such as displacements, velocities, and accelerations, are independent variables of the optimization problem together with the damping coefficients of the FVDs. The optimization algorithm treats the equations of motion as equality constraints. In this way, the equations of motions are not solved directly with time-history analyses. A major advantage of the proposed approach is that there is no need to calculate the gradients of the objective and constraint functions with design sensitivity analysis methods. During the optimization analysis, the equilibrium equations may not be satisfied. But once the optimization analysis is completed, we obtain the optimized values of the damping coefficients and the associated response quantities of the retrofitted structural system that satisfy the dynamic equilibrium equations. This approach is classified as a simultaneous analysis and design (SAND) optimization approach (Arora and Wang, 2005). SAND problem formulations in the literature are also called all-at-once or infeasible path formulations (Orozco and Ghattas, 1997).

In the literature, SAND approaches have been known since the 1960s. Schmit and Fox (1965) first presented a SAND approach in a structural engineering context. Since then, several authors have discussed SAND formulations for design optimization problems, e.g. (Haftka, 1985; Wu and Arora, 1987; Orozco and Ghattas, 1992; Larsson and Snnqvist, 1995; Ringertz, 1995; Stolpe and Svanberg, 2003; Wang and Arora, 2005, 2009; Iori, 2020). Recently, the author has briefly discussed a SAND approach for optimization-based seismic retrofitting of linear elastic structures with linear FVDs in Pollini (2023). Here, we present important steps forward with reference to Pollini (2023). A novel SAND approach is presented and discussed for the optimization of linear and nonlinear FVDs in seismic retrofitting applications of structures with inelastic behavior. As a result of initial numerical experiments, the problems at hand turn out to be challenging to solve within a single optimization analysis run. Thus, we also propose a procedure for solving a sequence of optimization sub-problems, where in every sub-problem relaxed but decreasing values of the design-driving inter-story drift constraints are considered. The solution obtained in every sub-problem is used as warm-start information for the subsequent sub-problem. The procedure stops when a solution that satisfies the desired value of the inter-story drift constraints is found. The numerical results show that the proposed SAND approach coupled with the continuation scheme for the drift constraints is capable of solving the challenging optimization problems considered here with modest computational resources.

In what follows, Sec. 2 describes the structural systems and the mechanical behaviors considered. The optimization problem formulations studied in this article are discussed in Sec. 3. The details of the computational tools and the framework developed are presented in Sec. 4, followed by numerical examples in Sec. 5. Sec. 6 concludes the article with final remarks.

2. Problem description

We consider the nonlinear structural systems shown in Fig. 1. These structures have two degrees of freedom, u_1 and u_2, and are subjected to a realistic ground acceleration. The masses m_1 and m_2 are equal to 25 t. The structure is defined by the mass matrix $\mathbf{M}$, the inherent damping matrix $\mathbf{C}$, and the initial stiffness matrix $\mathbf{K}_0$. We consider Rayleigh damping to define $\mathbf{C}$ (Chopra, 2012). The numerical entries of the system matrices are:

$$\mathbf{M} = \begin{bmatrix} 25 & 0 \\ 0 & 25 \end{bmatrix} 10^{-3}\, t,\ \mathbf{C} = \begin{bmatrix} 120.7 & -32.4 \\ -32.4 & 72.1 \end{bmatrix} 10^{-3}\, \frac{kNs}{mm},\ \mathbf{K}_{s0} = \begin{bmatrix} 62.5 & -25 \\ -25 & 25 \end{bmatrix} \frac{kN}{mm}. \tag{1}$$

In the optimization problem we constrain the values in time of the inter-story drifts of the structures considered. Inter-story drifts, in fact, are often used as an appropriate measure for both structural and nonstructural damage caused by

an earthquake (Lavan and Levy, 2006a; Pollini et al., 2017). The transformation from displacements $\mathbf{u}$ to inter-story drifts[1] $\mathbf{d}$ is done with the matrix $\mathbf{H}$:

$$\mathbf{d}(t_i) = \mathbf{H}\,\mathbf{u}(t_i), \quad \text{with } \mathbf{H} = \begin{bmatrix} 1 & 0 \\ -1 & 1 \end{bmatrix}, \tag{2}$$

for each time step t_i. We consider the first 20 s of the realistic ground motion record LA02 from the "LA 10% in 50 years" ground motions ensemble (Somerville, 1997). The ground acceleration record is plotted in Fig. 2. The record is defined in terms of discrete ground acceleration values $a_g(t_i)$, for $t_i = \{t_0, \ldots, t_{n_t}\}$ with n_t number of time steps.

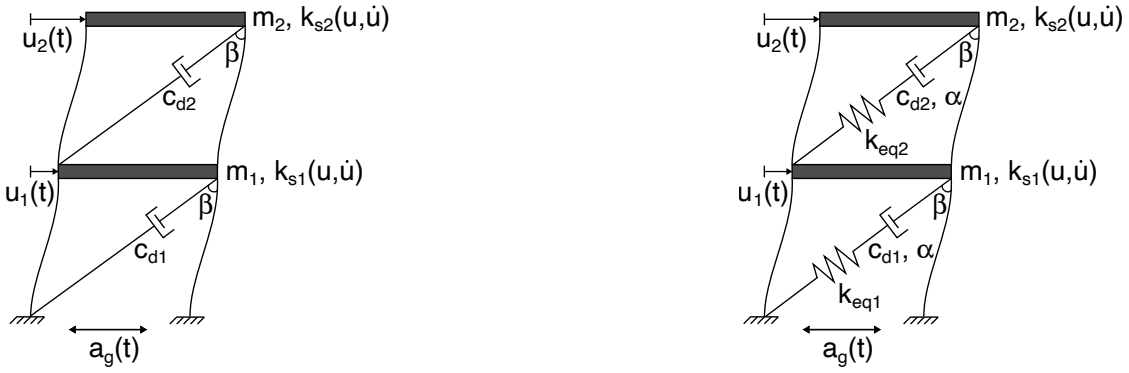

Figure 1: Nonlinear structural systems considered. Hysteretic structure retrofitted with linear (Fig. 1a), and nonlinear FVDs (Fig. 1b)

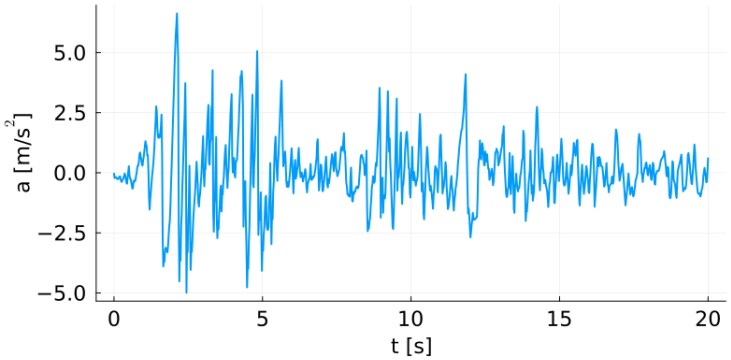

Figure 2: Ground acceleration record a_g considered. LA02 from the "LA 10% in 50 years" ground motions ensemble

The goal is to optimize the design of the added damping system, in this case made of two fluid viscous dampers. The associated design variables are the damping coefficients of the dampers, c_{d1} and c_{d2}, which are collected in the vector $\mathbf{c}_d$. We will consider two design cases. In the first case, linear dampers are optimized for a structure with nonlinear hysteretic behavior. In the second case, nonlinear dampers modelled with the Maxwell model are designed with the optimization approach proposed for retrofitting a structure with hysteretic nonlinear behavior.

Fluid viscous dampers are typically connected on one end to the structure and on the other to a supporting brace. In this work, when linear fluid viscous dampers are considered, the stiffnesses of the dampers and their supporting braces are not taken into account. A schematic presentation of the resulting structural system considered is shown in Fig. 1a. The added damping matrix $\mathbf{C}_d$ is

$$\mathbf{C}_d = \mathbf{H}^T \,\mathrm{diag}(\mathbf{c}_d)\,\mathbf{H} \tag{3}$$

[1] For inter-story drift we mean the relative displacement between the column ends

with diag() being an operator that transforms a vector into a diagonal matrix with the vector entries along the diagonal. The vector $\mathbf{c}_d$ contains the damping coefficients of each j-th damper: $\mathbf{c}_d = [c_d^1, \ldots, c_d^{n_d}]^T$. We predefine a maximum value of available damping that can be used in the design optimization process, $c_{d,max}$, and consider as design variables the vector with normalized damping coefficients $\mathbf{x}_d$, such that $c_d^j = c_{d,max}\, x_d^j$ with $0 \leq x_d^j \leq 1$ and $j = 1, \ldots, n_d$. In each time step t_i, the resisting force vector of the linear added damping system is:

$$\mathbf{F}_d(t_i) = \mathbf{C}_d\, \dot{\mathbf{u}}(t_i). \tag{4}$$

Recently, it was observed that considering a finite stiffness of the brace can significantly affect the mechanical behavior of the damper-brace (Akcelyan et al., 2016). Furthermore, today, researchers (Ji et al., 2013; Tubaldi et al., 2014, 2015; Parcianello et al., 2017; De Domenico and Ricciardi, 2018; Akcelyan et al., 2018; Altieri et al., 2018), engineers (Infanti et al., 2004), and producers (Taylor Devices; FIP MEC) consider viscous dampers with nonlinear force-velocity behavior. Thus, in the case of nonlinear dampers, we consider damper-brace systems made of two springs and a dashpot in series, as shown in Fig. 3. The first spring accounts for the stiffness of the supporting brace

Figure 3: Damper-brace Maxwell model

k_b, while the second spring accounts for the stiffness of the damper k_d. Lastly, the dashpot models the nonlinear force-velocity behavior of each fluid viscous damper. Its behavior is defined by the damping coefficient c_d, and the velocity exponent α. For a j-th damper-brace element at time-step t_i we have that:

$$\begin{aligned} F_{d,j}(t_i) &= k_{b,j}\, u_{d,j}(t_i), \\ F_{d,j}(t_i) &= k_{d,j}\, u_{d,j}(t_i), \\ F_{d,j}(t_i) &= c_{d,j}\, sign\left(\dot{u}_d(t_i)\right)\, |\dot{u}_d(t_i)|^{\alpha}, \end{aligned} \tag{5}$$

where $u_{d,j}(t_i)$ is the relative displacement in time between the damper-brace element ends. With respect to the structural system considered in the case of nonlinear FVDs, as shown in Fig. 1b, $u_{d,j}(t_i) = d_j(t_i)\, sin(\beta)$. The time derivative of the j-th damper-brace element at time-step t_i is defined as follows:

$$\dot{F}_{d,j}(t_i) = k_{eq,j}\left[\dot{d}_j(t_i)\, sin(\beta) \;-\; sign\left(F_{d,j}(t_i)\right)\left(\frac{\left|F_{d,j}(t_i)\right|}{c_{d,j}}\right)^{1/\alpha}\right]. \tag{6}$$

In Eq. 6, $k_{eq,j} = \rho\, c_{d,j}$ is the stiffness of the damper-brace element, and it accounts for the stiffness contribution of the damper and its supporting brace. The parameter ρ is predefined, and for more details on how to define it, the interested reader is referred to Pollini et al. (2017). The exponent α, which defines the nonlinear force-velocity relation of the dashpot is also predefined and set to 0.35. The angle β is defined as $\beta = asin\left(l/\sqrt{l^2 + h^2}\right)$, where $l = 5\ m$ is the length of each bay, and $h = 3\ m$ is the height of each story. All the damper-brace output forces $\dot{F}_{d,j}(t_i)$ are collected in the vector $\dot{\mathbf{F}}_d(t_i) = [\dot{F}_{d,1}(t_i), \ldots, \dot{F}_{d,n_d}(t_i)]^T$, where in this case the number of dampers is $n_d = 2$.

We consider a nonlinear hysteretic behavior of the horizontal resisting forces $F_{s,j}(t_i)$ for each j-th story. The hysteretic nonlinear behavior of the structure is modelled following Sivaselvan and Reinhorn (2000):

$$\dot{F}_{s,j}(t_i) = k_{s0,j}\left\{a + [1-a]\left[1 - \left|\frac{F^*_{s,j}(t_i)}{F^*_{y,j}}\right|^n \left(0.5\, sign\left(F^*_{s,j}(t_i)\, \dot{d}_j(t_i)\right) + 0.5\right)\right]\right\}. \tag{7}$$

In Eq. 7, $k_{s0,j}$ is the initial stiffness (in drift coordinates, see Eq. (2)) of the j-th story:

$$\mathbf{k}_{s0} = \begin{bmatrix} 37.5 \\ 25.0 \end{bmatrix} \text{ kN/mm}. \tag{8}$$

The parameter a defines the percentage of initial stiffness available in the post-yield region, and n controls the sharpness of the transition from initial to post-yield stiffness. Moreover, $F^*_{s,j}(t_i) = F_{s,j}(t_i) - a\, k_{s0,j}\, d_j(t_i)$ and $F^*_{y,j} = (1-a)\, F_{y,j}$, (Sivaselvan and Reinhorn, 2000). All structural internal forces $\dot{F}_{s,j}(t_i)$ are collected in the vector $\dot{\mathbf{F}}_s(t_i) = [\dot{F}_{s,1}(t_i), \ldots, \dot{F}_{s,n_s}(t_i)]^T$, where in this case the number of stories is $n_s = 2$.

We adopt the Newmark-β average acceleration approach to define the equations of motion, which are treated as equality constraints in the optimization problem. Considering the definition $\mathbf{u}_i \equiv \mathbf{u}(t_i)$ (and similarly for the other response quantities), the equations of motion read:

$$\mathbf{M}\ddot{\mathbf{u}}_i + \mathbf{C}\dot{\mathbf{u}}_i + \mathbf{H}^T\,\mathbf{F}_{di}\, sin(\beta) + \mathbf{H}^T\,\mathbf{F}_{si} + a_{g,i}\mathbf{M}\mathbf{e} = \mathbf{0} \tag{9a}$$

$$-\,\mathbf{u}_{i+1} + \mathbf{u}_i + \Delta t\,\dot{\mathbf{u}}_i + \Delta t^2\left(\frac{1}{2} + \beta\right)\ddot{\mathbf{u}}_i + \Delta t^2\,\beta\,\ddot{\mathbf{u}}_{i+1} = 0 \tag{9b}$$

$$-\,\dot{\mathbf{u}}_{i+1} + \dot{\mathbf{u}}_i + (1-\gamma)\,\Delta t\,\ddot{\mathbf{u}}_i + \gamma\,\Delta t\,\ddot{\mathbf{u}}_{i+1} = 0 \tag{9c}$$

$$\mathbf{u}_0 = \mathbf{0},\ \dot{\mathbf{u}}_0 = \mathbf{0},\ \mathbf{F}_{s0} = \mathbf{0},\ \mathbf{F}_{d0} = \mathbf{0} \tag{9d}$$

$$\tag{9e}$$

with $\mathbf{e} = [1\ 1]^T$, $\beta = 0.25$, and $\gamma = 0.5$. Eq. (9) are written in a more compact form as $\mathbf{R}_{eq}(\mathbf{u}_i, \dot{\mathbf{u}}_i, \ddot{\mathbf{u}}_i, \mathbf{F}_{d,i}, \mathbf{F}_{s,i}) = \mathbf{0}$.

We will consider two design scenarios. In the first, defined in problem ($\mathcal{P}_1$), we consider the structural system depicted in Fig. 1a. It consists of a two-story frame with nonlinear hysteretic force-displacement behavior, and equipped with linear fluid viscous dampers (Eq.4) whose stiffening contribution is not accounted for. In the second, defined in ($\mathcal{P}_2$), we consider the structural system depicted in Fig. 1b. It consists of a two-story frame with nonlinear hysteretic force-displacement behavior and equipped with nonlinear fluid viscous dampers (Eq.6), where we consider also the stiffness contribution of each damper and its supporting brace.

3. Optimization problem formulations

In this section we provide the details of the two optimization problem formulations considered. As mentioned previously, the first formulation refers to the first design scenario, $\mathcal{P}_1$: a nonlinear hysteretic structure equipped with linear dampers. In similar retrofitting design problems (Shin and Singh, 2014a,b; Gidaris and Taflanidis, 2015), the life-cycle cost has been taken as the objective function to be minimized. In the approach discussed herein, we minimize a component of the initial retrofitting cost, the dampers' manufacturing cost. This is proportional to the maximum force that the dampers experience, and hence they are designed for (Pollini et al., 2017). We thus minimize the maximum force of the dampers by minimizing a fictitious variable τ, which acts also as upper variable limit for the constraints on the absolute value of each j-th damper force in each i-th time step:

$$\left|F^j_{d,i}\right| \leq \tau. \tag{10}$$

Lastly, we constrain a performance index related to both structural and nonstructural damage caused by an earthquake, the inter-story drifts (Lavan and Levy, 2006a). We constrain their maximum value in time by introducing the following constraints:

$$-d_{max} \leq \mathbf{d}_i \leq d_{max}. \tag{11}$$

Thus, for each time step t_i with $i = 1, \ldots, n_t$, damper index $j = 1, \ldots, n_d$, and story index $k = 1, \ldots, n_s$ the first

optimization problem is formulated as follows:

$$
\begin{aligned}
\underset{\bar{\mathbf{x}} \in \Phi}{\text{minimize}} \quad & \tau \\
\text{subject to} \quad & \left| F_{d,i}^{j} \right| \leq \tau \\
& -d_{max} \leq \mathbf{d}_i \leq d_{max} \\
& \mathbf{d}_i = \mathbf{H}\,\mathbf{u}_i \\
& \dot{\mathbf{d}}_i = \mathbf{H}\,\dot{\mathbf{u}}_i \\
& \mathbf{F}_{d,i} = \mathbf{C}_d\,\dot{\mathbf{u}}_i \\
& F_{s,i}^{k} = F_{s,i-1}^{k} + \dot{F}_{s,i-1}^{k}\,\Delta t \\
& \dot{F}_{s,i}^{k} = k_{s0}^{k} \left\{ a + [1-a] \left[1 - \left| \frac{F_{s,i}^{*k}}{F_{y}^{*k}} \right|^{n} \left(0.5\; sign\left(F_{s,i}^{*k}\,\dot{d}_i^{k} \right) + 0.5 \right) \right] \right\} \\
& \mathbf{R}_{eq}(\mathbf{u}_i, \dot{\mathbf{u}}_i, \ddot{\mathbf{u}}_i, \mathbf{F}_{d,i}, \mathbf{F}_{s,i}) = \mathbf{0}
\end{aligned}
\tag{$\mathcal{P}_1$}
$$

In ($\mathcal{P}_1$), the vector $\bar{\mathbf{x}}$ contains all the optimization variables. These are:

$$
\bar{\mathbf{x}} = \left\{ \tau, \mathbf{x}_d, \mathbf{u}, \dot{\mathbf{u}}, \ddot{\mathbf{u}}, \mathbf{d}, \dot{\mathbf{d}}, \mathbf{F}_d, \mathbf{F}_s, \dot{\mathbf{F}}_s \right\}. \tag{12}
$$

The set Φ is the set of points $\bar{\mathbf{x}}$ such that:

$$
\begin{aligned}
\Phi = \Big\{ \bar{\mathbf{x}} \;\mid\; & \tau \in \mathbb{R} \text{ and } 0 \leq \tau, \mathbf{x}_d \in \mathbb{R}^{n_d} \text{ and } 0 \leq \mathbf{x}_d \leq 1, \mathbf{u} \in \mathbb{R}^{n_u \times n_t}, \dot{\mathbf{u}} \in \mathbb{R}^{n_u \times n_t}, \ddot{\mathbf{u}} \in \mathbb{R}^{n_u \times n_t}, \\
& \mathbf{d} \in \mathbb{R}^{n_d \times n_t}, \dot{\mathbf{d}} \in \mathbb{R}^{n_d \times n_t}, \mathbf{F}_d \in \mathbb{R}^{n_d \times n_t}, \mathbf{F}_s \in \mathbb{R}^{n_s \times n_t}, \dot{\mathbf{F}}_s \in \mathbb{R}^{n_s \times n_t - 1} \Big\}
\end{aligned}
\tag{13}
$$

where n_d is the number of dampers being optimized which equals the number of inter-story drifts constrained in our case; n_u is the number of degrees of freedom of the structure; n_t is the number of time steps; n_s is the number of stories of the structure.

The second formulation refers to the second design scenario, $\mathcal{P}_2$: a nonlinear hysteretic structure equipped with nonlinear dampers. In its formulation, $\mathcal{P}_2$ is quite similar to that of $\mathcal{P}_1$. The main difference are the equations that define the behavior in time of the nonlinear fluid viscous dampers. Thus, for time steps t_i with $i = 1, \ldots, n_t$, and damper index $j = 1, \ldots, n_d$, and story index $k = 1, \ldots, n_s$ the second optimization problem is formulated as follows:

$$
\begin{aligned}
\underset{\bar{\mathbf{x}} \in \Psi}{\text{minimize}} \quad & \tau \\
\text{subject to} \quad & \left| F_{d,j}^{i} \right| \leq \tau \\
& -d_{max} \leq \mathbf{d}_i \leq d_{max} \\
& \mathbf{d}_i = \mathbf{H}\,\mathbf{u}_i \\
& \dot{\mathbf{d}}_i = \mathbf{H}\,\dot{\mathbf{u}}_i \\
& F_{d,i}^{j} = F_{d,i-1}^{j} + \dot{F}_{d,i-1}^{j}\,\Delta t \\
& \dot{F}_{d,i}^{j} = k_{eq}^{j} \left[\dot{d}_i^{j}\; sin(\beta) \;-\; sign\left(F_{d,i}^{j} \right) \left(\frac{\left| F_{d,i}^{j} \right|}{c_d^{j}} \right)^{1/\alpha} \right] \\
& F_{s,i}^{k} = F_{s,i-1}^{k} + \dot{F}_{s,i-1}^{k}\,\Delta t \\
& \dot{F}_{s,i}^{k} = k_{s0}^{k} \left\{ a + [1-a] \left[1 - \left| \frac{F_{s,i}^{*k}}{F_{y}^{*k}} \right|^{n} \left(0.5\; sign\left(F_{s,i}^{*k}\,\dot{d}_i^{k} \right) + 0.5 \right) \right] \right\} \\
& \mathbf{R}_{eq}(\mathbf{u}_i, \dot{\mathbf{u}}_i, \ddot{\mathbf{u}}_i, \mathbf{F}_{d,i}, \mathbf{F}_{s,i}) = \mathbf{0}
\end{aligned}
\tag{$\mathcal{P}_2$}
$$

In ($\mathcal{P}_2$), the vector $\tilde{\mathbf{x}}$ contains all the optimization variables. These are:

$$\tilde{\mathbf{x}} = \left\{\tau, \mathbf{x}_d, \mathbf{u}, \dot{\mathbf{u}}, \ddot{\mathbf{u}}, \mathbf{d}, \dot{\mathbf{d}}, \mathbf{F}_d, \dot{\mathbf{F}}_d, \mathbf{F}_s, \dot{\mathbf{F}}_s\right\}. \tag{14}$$

The set Ψ is the set of points $\tilde{\mathbf{x}}$ such that:

$$\begin{aligned}\Psi = \Big\{\tilde{\mathbf{x}} \;\mid\; & \tau \in \mathbb{R} \text{ and } 0 \leq \tau, \mathbf{x}_d \in \mathbb{R}^{n_d} \text{ and } 0 \leq \mathbf{x}_d \leq 1, \mathbf{u} \in \mathbb{R}^{n_u \times n_t}, \dot{\mathbf{u}} \in \mathbb{R}^{n_u \times n_t}, \ddot{\mathbf{u}} \in \mathbb{R}^{n_u \times n_t}, \\ & \mathbf{d} \in \mathbb{R}^{n_d \times n_t}, \dot{\mathbf{d}} \in \mathbb{R}^{n_d \times n_t}, \mathbf{F}_d \in \mathbb{R}^{n_d \times n_t}, \dot{\mathbf{F}}_d \in \mathbb{R}^{n_d \times n_t - 1}, \mathbf{F}_s \in \mathbb{R}^{n_s \times n_t}, \dot{\mathbf{F}}_s \in \mathbb{R}^{n_s \times n_t - 1}\Big\}.\end{aligned} \tag{15}$$

The specific values of the parameters that define problems ($\mathcal{P}_1$) and ($\mathcal{P}_2$), and that were considered in the numerical examples, are given in Sec. 4 and Sec. 5.

4. Computational considerations

The optimization problems are all implemented in Julia version 1.9.1 (Bezanson et al., 2017; The Julia Project, 2023). The nonlinear optimization problems $\mathcal{P}_1$ and $\mathcal{P}_2$ are modeled with JuMP (Lubin et al., 2023), a mathematical optimization modeling language for the Julia programming language. The optimization problems are solved numerically with the interior-point algorithm IPOPT version 3.14.13 (Wächter and Biegler, 2006) with the linear solver MUMPS version 5.6.0, which is available in Julia through the package Ipopt.jl (JuMP community, 2023). The analytical gradients of the objective and constraint functions are computed numerically with the automatic differentiation capabilities embedded in JuMP.

The optimization problems are scaled to allow for a more robust and stable performance of the optimization solver. In particular, as a result of initial numerical experiments, the optimization variables $\dot{\mathbf{u}}_i$ are scaled by a factor of 10, and the optimization variables $\ddot{\mathbf{u}}_i$ are scaled by a factor of 10^2. Moreover, in problem ($\mathcal{P}_1$) the variables $\mathbf{F}_{d,i}$ are scaled by a factor of $10\, c_{d,max}$, whereas in problem ($\mathcal{P}_2$) the variables $\mathbf{F}_{d,i}$ and $\dot{\mathbf{F}}_{d,i}$ are scaled by a factor of 10 only. In both problems, the variables $\mathbf{F}_{s,i}$ and $\dot{\mathbf{F}}_{s,i}$ and the equations of motion (9a) are scaled by a factor of 10. Table 1 summarizes the scaling factor considered. The scaling option available in the optimization solver IPOPT is disabled.

During initial numerical experiments, it became clear that the optimization problems at hand are quite challenging to solve numerically. This is particularly true in the case of problem ($\mathcal{P}_2$). One reason is that the optimization problems are very large (in terms of number of optimization variables; more details are given in Sec. 5). This is something intrinsic for SAND optimization approaches, but in the design cases considered here, this is even more significant due to the fact that the optimization response variables vary in time. Another reason is that in the optimization process, all design and response variables are automatically initialized by the optimization solver, and it takes several iterations until feasible solutions are identified. In order to alleviate this difficulty, we propose a continuation scheme for the value of the predefined maximum allowed inter-story drift. The design-driving drift constraints (Eq. (11)) are relaxed and then tightened progressively defining in this way sequences of sub-problems that are easier to solve for the optimization algorithm. The solutions thus obtained in each sub-problem are then used as warm-start information in the subsequent optimization analyses, which have tighter bounds for the drift constraints. This procedure is repeated until a solution is found that satisfies all drift constraints with the actual maximum allowed inter-story drift value, as shown in Algorithm 1.

5. Numerical examples

In the following section, we present the numerical results obtained by solving the optimization problems ($\mathcal{P}_1$) and ($\mathcal{P}_2$). The optimization analyses are run on a computer running Windows 11, with 32 Gb of RAM, and a 12th-gen Intel (R) Core (TM) i7 CPU running at 4.7 GHz. With IPOPT, the following settings were adopted:

- `hessian_approximation` set to `limited-memory`;
- `linear_solver` set to `mumps`;
- `expect_infeasible_problem` set to `no`;

Algorithm 1: Algorithm for sequential solution of $(\mathcal{P}_1)$ and $(\mathcal{P}_2)$ with varying drift constraint limit and use of warm-start information

Define $\mathbf{d}_{vec} = [d_{max,1}, \ldots, d_{max,n}]$, $d_{max,n}$ is the actual limit that we want to impose.
Note: $d_{max,1} > d_{max,2} > \cdots > d_{max,n}$.
for $k = 1 : length(\mathbf{d}_{vec})$ **do**
  Set $d_{max} = \mathbf{d}_{vec}[k]$ in Eq. (11).
  Solve problem $(\mathcal{P}_1)^k$ or $(\mathcal{P}_2)^k$.
  Set $\mathbf{x}_0 = \mathbf{x}_{opt}^k$ as warm-start information for IPOPT in $(\mathcal{P}_1)^{k+1}$ or $(\mathcal{P}_2)^{k+1}$.
end
Let $\mathbf{x}_{opt}^{final} = \mathbf{x}_{opt}^k$.

Optimization variable	Description	Scaling
$\mathbf{u}_i$	displacements	1
$\dot{\mathbf{u}}_i$	velocities	10
$\ddot{\mathbf{u}}_i$	accelerations	10^2
$\mathbf{F}_{s,i}$	structural restoring forces	10
$\dot{\mathbf{F}}_{s,i}$	time derivative of structural restoring forces	10
$\mathbf{F}_{d,i}$	damper forces	$c_{d,max}10$ $(\mathcal{P}_1)$, 10 $(\mathcal{P}_2)$
$\dot{\mathbf{F}}_{d,i}$	time derivative of damper forces	$c_{d,max}10$ $(\mathcal{P}_1)$, 10 $(\mathcal{P}_2)$

Table 1: Scaling factors of the optimization variables

- `max_iter` set to 500;
- `tol` set to 10^{-6};
- `constr_viol_tol` set to 10^{-6};
- `acceptable_tol` set to $5 \cdot 10^{-5}$;
- `acceptable_constr_viol_tol` set to $5 \cdot 10^{-5}$.

For both problems, we run a sequence of optimization analyses, where the solution found at the end of each optimization analysis serves as a starting point in the subsequent analysis. In each optimization analysis a different value of maximum allowed inter-story drift is considered in Eq. (11), starting from a higher value down to a desired value (see Algorithm (1)). In particular, the following sequence of values is considered for the parameter d_{max}: $\mathbf{d}_{vec} = [15.0, 13.0, 11.0, 9.0]$ mm. In Eq. (6) $\alpha = 0.35$ and $\rho = 1.1042$. The structural hysteretic behavior governed by Eq. (7) is defined by setting $n = 5$, $a = 5\%$, and $\mathbf{F}_y = [169.0, 107.0]^T$ kN.

5.1. Hysteretic structure with linear fluid viscous dampers

We first discuss the results obtained solving problem $\mathcal{P}_1$, which is associated with the structural system shown in Fig. 1a. The problem consists in optimizing the size and placement of linear FVDs placed in a structure with nonlinear hysteretic behavior. We discretize the loading, and as a consequence the system response, with constant time steps $\Delta t = 0.006$ s, and a number of time steps $n_t = 3\,334$. Thus, the resulting problem has 53 345 optimization variables, 53 342 equality constraints, and 6 666 inequality constraints. In this case, the value of the maximum available damping coefficient is set to $c_{d,max} = 5$ kN$\frac{\text{s}}{\text{mm}}$. The optimization analysis converged after a total of 109 iterations in 24 s. The final optimized solution consists of damping coefficients $c_{d1} = 2.96$ kN$\frac{\text{s}}{\text{mm}}$ and $c_{d2} = 0.92$ kN$\frac{\text{s}}{\text{mm}}$. The final value of the objective function is $\tau^{opt} = 238.19$ kN, which at the final optimal point is equal to the maximum force value in time of the most loaded damper $F_{d,max}$.

Since we applied a continuation scheme on the maximum allowed inter-story drift value d_{max} (see Algorithm 1), a sequence of four optimization sub-problems was solved. This was done in order to obtain the final optimized solution

reported above. The optimization solver was unable to solve the desired problem formulation ($\mathcal{P}_1$) with d_{max} = 9 mm in a single optimization analysis run. Fig. 4 shows the optimized damping coefficients (Fig. 4a) and objective function values (Fig. 4b) obtained at the end of each intermediate sub-problem. Table 2 reports the numerical results shown in Fig. 4, together also with the number of iterations and computational time required by IPOPT for solving each sub-problem. We can observe that as we reduce the value of the maximum inter-story drift allowed, the values of the optimized damping coefficients increase monotonically. At the same time, the final optimized value of the objective function (which at the end of each optimization analysis is equal to the maximum output force in time of the most loaded damper) also increases. This happens because, for decreasing values of maximum inter-story drift allowed, we need an added damping system capable of producing output resisting forces with higher maximum absolute values in order to control the structural response accordingly. Sub-problem 1 (with d_{max} = 15 mm in Table 2) requires the highest number of iterations. This may be due to the fact that only in this case the optimization variables are initialized by the optimization solver IPOPT. However, this is a speculative statement of the author. In the other subsequent sub-problems, the optimization variables are initialized using the optimal values obtained in the preceding sub-problem. These initial values are closer to the final optimal values and therefore the solver converges with fewer iterations to the final solution.

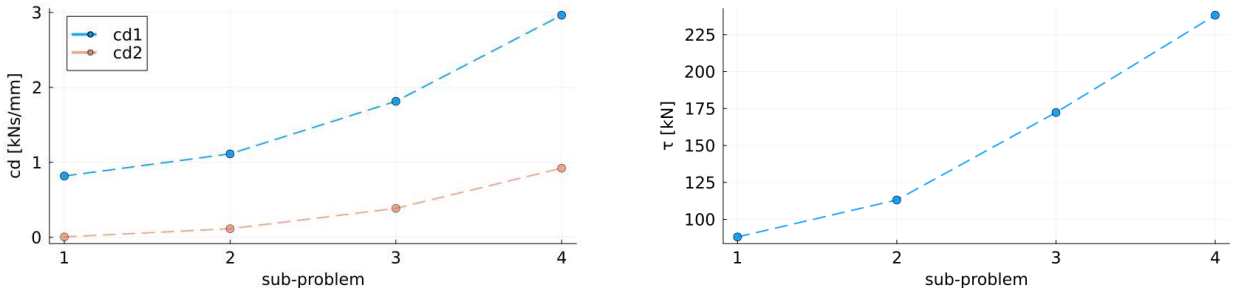

(a) (b)

Figure 4: Evolution of the optimized solutions obtained solving problem $\mathcal{P}_1$ as a sequence of sub-problems for varying values of d_{max}. Optimized damping coefficient values c_{d1} and c_{d2} (4a) and objective function values τ (4b)

Sub-problem	d_{max} [mm]	c_{d1} [kNs/mm]	c_{d2} [kNs/mm]	τ [kN]	Iterations [#]	Time [s]
1	15.0	0.82	0.01	88.11	37	6.0
2	13.0	1.11	0.11	113.13	15	4.1
3	11.0	1.81	0.39	172.33	23	5.9
4	9.0	2.96	0.92	238.19	34	7.9

Table 2: Optimized solutions obtained solving problem ($\mathcal{P}_1$) sequentially for varying values of of maximum inter-story drift allowed d_{max}, as described in Algorithm 1

Fig. 5 shows the optimized response of the retrofitted structure. In particular, Fig. 5a shows the inter-story drift response. The dashed line marks the maximum drift allowed (9 mm). It can be observed that the response does not exceed the constraint limit in any of the time steps, as expected. Fig. 5b shows the optimized response of the retrofitted structure but in this case in terms of displacements $\mathbf{u}(t_i)$ rather than drifts $\mathbf{d}(t_i)$.

The force-displacement plots of the optimized dampers and of the structure internal forces are shown in Fig. 6 and Fig. 7. In Fig. 6 we observe the known hysteretic behavior of linear FVDs. The most loaded damper is the bottom one, with associated damping coefficient c_{d1} (Fig. 6a). In Fig. 7 we recognize the expected hysteretic behavior of the structure, where in the presence of yielding the structural stiffness significantly decreases.

5.2. Hysteretic structure with nonlinear fluid viscous dampers

We now discuss the results obtained solving problem $\mathcal{P}_2$, which is associated to the structural system shown in Fig. 1b. It consists in optimizing nonlinear FVDs placed in a structural system with nonlinear hysteretic behavior.

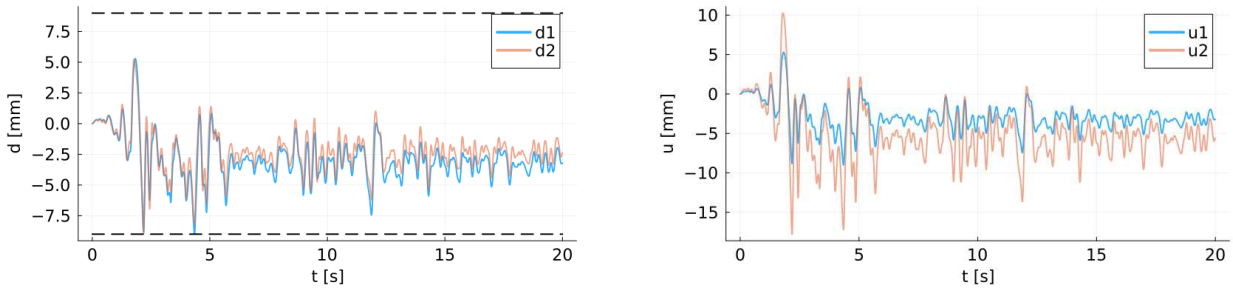

(a) (b)

Figure 5: Optimized structural response obtained solving problem $\mathcal{P}_1$. Drifts d (5a) and displacements u (5b). The dashed line in 5a indicates the maximum allowed inter-story drift value $d_{max} = 9$ mm

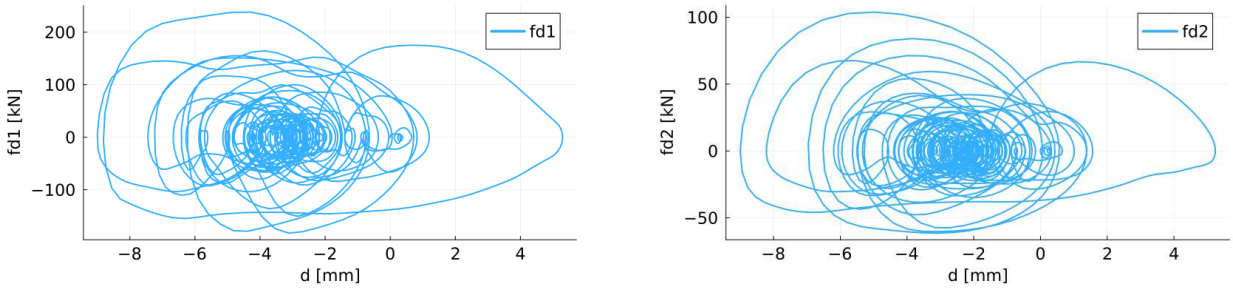

(a) (b)

Figure 6: Optimized dampers' forces F_{d1} (6a) and F_{d2} (6b) obtained solving problem $\mathcal{P}_1$

Now we discretize the loading, and as a consequence the system response, with constant time step sizes $\Delta t = 0.002$ s, and a number of time steps $n_t = 10\,001$. The problem considered now has 180 017 optimization variables, 180 014 equality constraints, and 20 000 inequality constraints. In this case, the maximum damping coefficient value is set to $c_{d,max} = 100\ \text{kN}\left(\frac{\text{s}}{\text{mm}}\right)^{\alpha}$. The optimization analysis converged after 526 iterations in 389 s. The optimized solution consists of the damping coefficients $c_{d1} = 34.57\ \text{kN}\left(\frac{\text{s}}{\text{mm}}\right)^{\alpha}$ and $c_{d2} = 28.18\ \text{kN}\left(\frac{\text{s}}{\text{mm}}\right)^{\alpha}$. The final value of the objective function is $\tau^{opt} = 173.55$ kN, which in this case is equal to the maximum force value of the most loaded damper $F_{d,max}$.

Also in this example, we applied a continuation scheme on the maximum allowed inter-story drift value d_{max} (see Algorithm 1). We did it first to be able to obtain a final solution as the one reported above and second to be able to

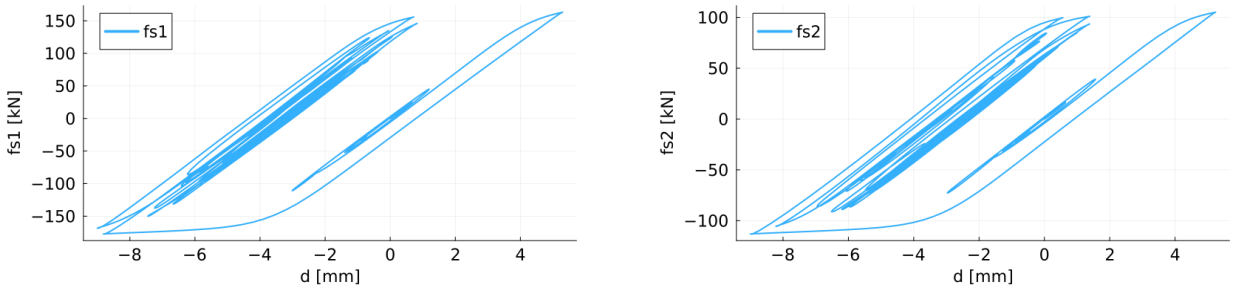

(a) (b)

Figure 7: Optimized structural responses F_{s1} (7a) and F_{s2} (7b) obtained solving problem $\mathcal{P}_1$

obtain it in a stable manner, from a computational point of view. We remark that during initial numerical experiments, it became clear that also in this case the optimization algorithm was not able to reach a feasible solution in just one optimization analysis. As a result, the only way to find a design solution was to use the sequential optimization approach outlined in Algorithm 1. Fig. 8 shows the optimized damping coefficients (Fig. 8a) and objective function (Fig. 8b) values obtained at the end of each intermediate sub-problem. We report the numerical results shown in Fig. 8 in Table 3, which also includes the number of iterations and computational time required by IPOPT for solving each sub-problem. We can observe also in this case that as we reduce the value of the maximum inter-story drift allowed, the values of the optimized damping coefficients increase monotonically. At the same time, the final optimized value of the objective function, and hence of the maximum damper force in time, also increases. As the maximum inter-story drift allowed decreases, the maximum output force needed to control the structural response increases accordingly. Nevertheless, in this case, we observe that in each sub-problem the maximum damper force needed to control the structural system with nonlinear FVDs is lower than that needed in the case of linear FVDs. The benefits associated with this aspect are twofold. On the one hand, since the cost of FVDs is proportional to the peak force for which they are designed, having FVDs designed for lower maximum values of output force can be convenient from an economical point of view. However, FVDs that produce lower peak forces compared to linear FVDs in the same design scenario could be beneficial from a mechanical point of view. In fact, the forces produced by FVDs to control the structural response act as resisting forces on the structural elements, and this may cause an increase in the stress and deformation levels of structural elements, such as beams and columns, whose integrity is critical during an earthquake.

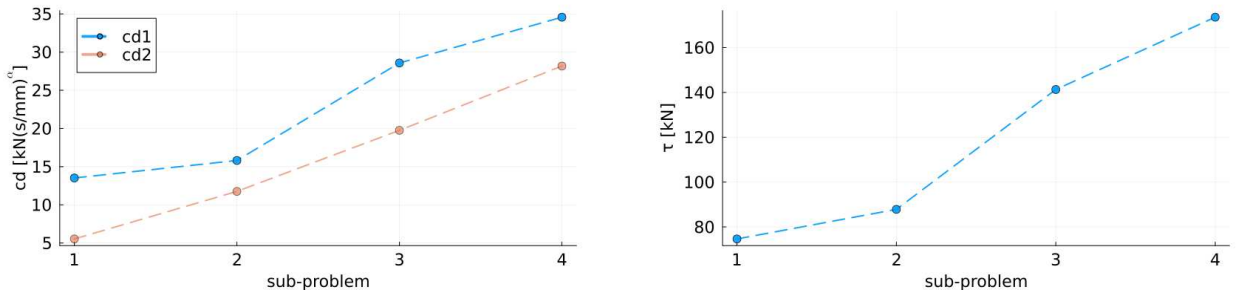

(a) (b)

Figure 8: Evolution of the optimized solutions obtained solving problem $\mathcal{P}_2$ as a sequence of sub-problems for varying values of d_{max}. Optimized damping coefficients c_{d1} and c_{d2} (8a) and objective function τ (8b)

Sub-problem	d_{max} [mm]	c_{d1} [kN(s/mm)$^\alpha$]	c_{d2} [kN(s/mm)$^\alpha$]	τ [kN]	Iterations [#]	Time [s]
1	15.0	13.52	5.53	74.63	100	84.4
2	13.0	15.81	11.76	87.83	131	83.5
3	11.0	28.58	19.76	141.29	247	186.2
4	9.0	34.57	28.18	173.55	48	34.5

Table 3: Optimized solutions obtained solving problem ($\mathcal{P}_2$) sequentially for varying values of maximum inter-story drift allowed d_{max}, as described in Algorithm 1

Fig. 9 shows the optimized response of the retrofitted structure. In particular, Fig. 9a shows the optimized drift response. The dashed line marks the maximum drift allowed (9 mm). It can be observed that the response does not exceed the constraint limit in any of the time steps, as expected. Fig. 9b shows the optimized response of the retrofitted structure but this time in terms of displacements $\mathbf{u}(t_i)$ rather than drifts $\mathbf{d}(t_i)$.

In this case, we report the force-velocity plots of the optimized dampers (Fig. 10) and the force-displacement plots of the internal forces of the structure (Fig. 11). In Fig. 10 we observe the known hysteretic force-velocity behavior of nonlinear FVDs. The most loaded damper is the bottom one, with associated damping coefficient c_{d1}. Nevertheless, in this case the two dampers experience a peak force more similar in magnitude, compared to the linear FVDs case, where the peak force of the first damper (F_{d1}) is significantly higher than that of the second damper (F_{d2}).

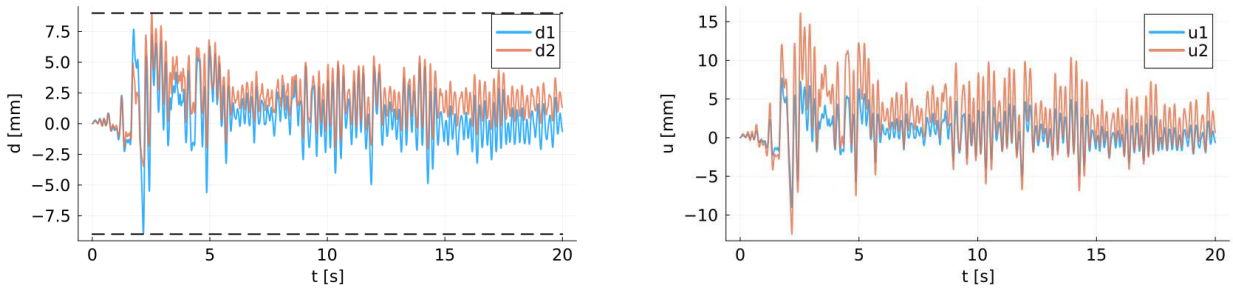

(a) (b)

Figure 9: Optimized structural response. Drifts d (9a) and displacements u (9b). The dashed line in 9a indicates the maximum allowed inter-story drift value $d_{max} = 9$ mm

In Fig. 11 we recognize once more the expected hysteretic behavior of the structure where, in the presence of yielding, the structural stiffness significantly decreases. Additionally, if we compare Fig. 5b and Fig. 9b we can see that the structure equipped with linear FVDs has higher residual displacements at the end of the seismic excitation than the structure with nonlinear FVDs. At this stage, it is not possible to determine whether this is a characteristic that applies universally to linear and nonlinear FVDs. However, it may be worth researching more about this aspect.

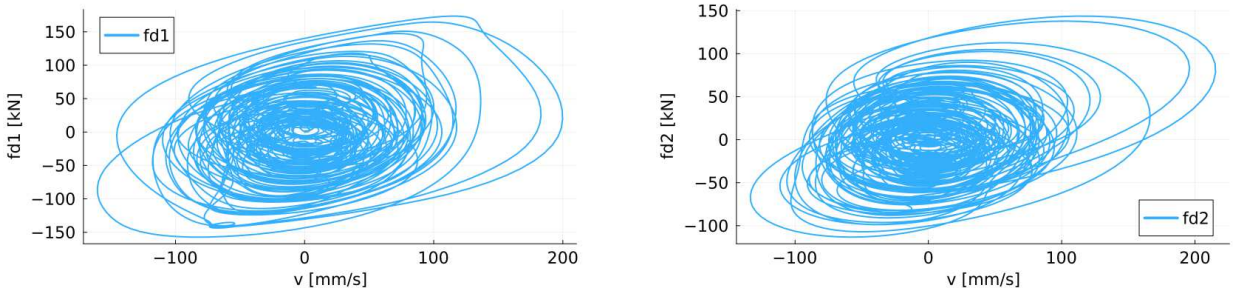

(a) (b)

Figure 10: Optimized dampers' forces F_{d1} (10a) and F_{d2} (10b) obtained solving problem $\mathcal{P}_2$. In the figures, $v \equiv \dot{d}$

5.3. Adding constraints

One of the advantages of SAND optimization approaches compared to more traditional gradient-based NAND optimization approaches is their modelling flexibility. This is particularly valuable when adding new response constraints to the formulation and implementation of a given optimization problem. In the case of gradient-based NAND approaches, new constraints often mean new adjoint, or direct, sensitivity analyses. These often require complicated analytical derivations that need to be programmed and then verified numerically, typically against finite-difference gradient computations. In the case of SAND approaches, instead, adding new constraints in many cases is much simpler because all the response quantities are treated as independent optimization variables. Therefore, it is possible to impose additional constraint on the system response directly in the form of box constraints or explicit functions.

We now want to address this aspect with an additional numerical example. We base our discussion on problem ($\mathcal{P}_1$), and Fig. 1a. However, this time we consider 30% of the initial stiffness in the post-yielding phase, i.e. $a = 30\%$ in Eq. (7). Thus, we first solve the same problem as in Sec. 5.1 with the only difference being the value assigned to the parameter a in Eq. (7), $a = 30\%$. We discretize the loading with constant time steps $\Delta t = 0.004$ s, leading to a number of time steps $n_t = 5\,001$. The problem considered now has 80 017 optimization variables, 80 014 equality constraints, and 10 000 inequality constraints. In this case, the maximum damping coefficient value is set to $c_{d,max} = 5$ kN$\frac{\text{s}}{\text{mm}}$. The optimization analysis converged with 135 iterations in 48 s. The optimized solution consists of damping coefficients $c_{d1} = 2.72$ kN$\frac{\text{s}}{\text{mm}}$ and $c_{d2} = 0.73$ kN$\frac{\text{s}}{\text{mm}}$. The final value of the objective function is $\tau^{opt} = 257.06$ kN.

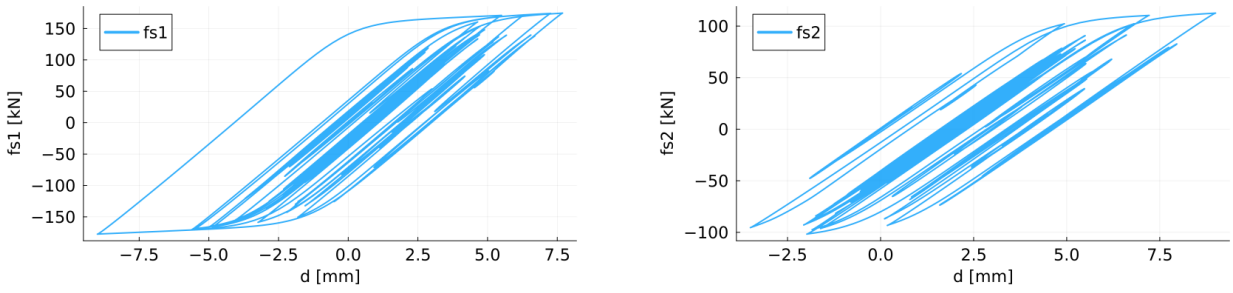

(a) (b)

Figure 11: Optimized structural responses F_{s1} (11a) and F_{s2} (11b) obtained solving problem $\mathcal{P}_2$

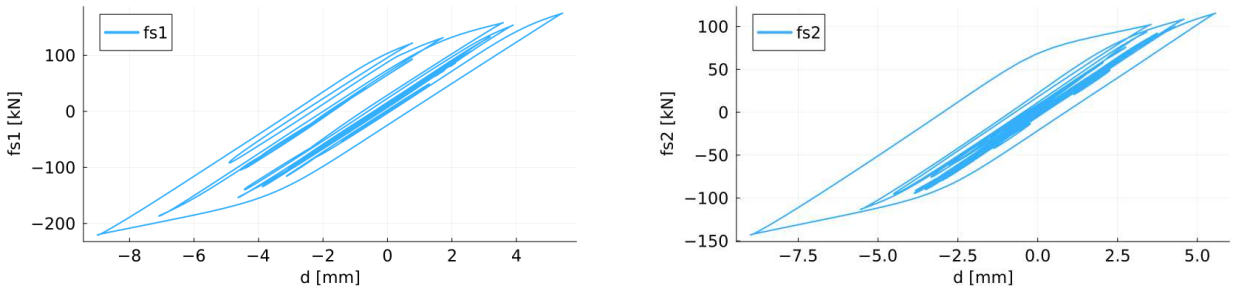

(a) (b)

Figure 12: Optimized structural responses F_{s1} (12a) and F_{s2} (12b) obtained solving problem $\mathcal{P}_1$ while considering 30% of the initial stiffness in the post-yielding phase (i.e. $a = 30\%$ in Eq. (7))

Fig. 12 shows the structural force-displacement plots associated with the optimized design obtained for the FVDs. The different behavior in the post-yielding phase can be observed due to the higher value considered for the parameter a.

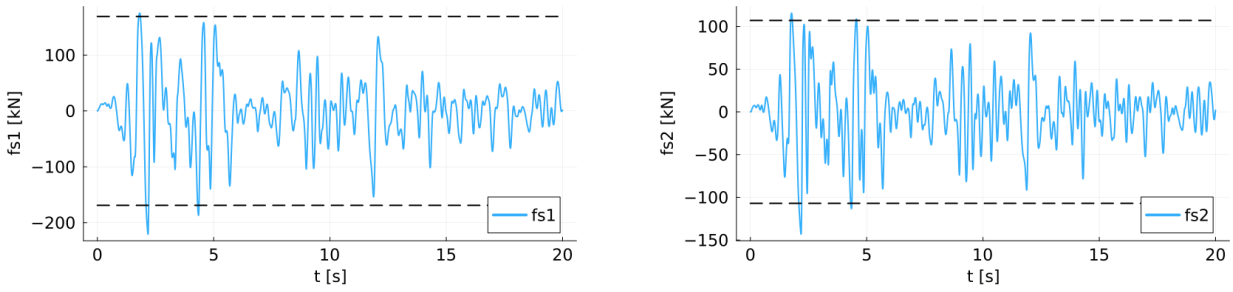

(a) (b)

Figure 13: Optimized structural responses F_{s1} (13a) and F_{s2} (13b) obtained solving problem $\mathcal{P}_1$ while considering 30% of the initial stiffness in the post-yielding phase (i.e. $a = 30\%$ in Eq. (7)). The dashed lines represent the yielding forces' values $F_{y,1} = 169.0$ kN and $F_{y,2} = 107.0$ kN

Fig. 13, instead, shows the structural force time-history plots associated with the optimized design obtained. The dashed lines mark the yielding limits, that are $F_{y,1} = 169.0$ kN and $F_{y,2} = 107.0$ kN. It can be observed that in few time-steps the structural forces exceed the yielding limit. This happen when the structure goes into post-yielding states.

Let us now assume that we want to find an optimized design for the FVDs such that the structural response remains within the elastic range. In this way, we significantly decrease the deformation demand on the structure, reducing the

amount of energy dissipated by the structural members. We can achieve this by constraining the values of the structural force variables $F_{s,1}$ and $F_{s,2}$. In particular, for each j-th structural force in each i-th time-step we add the following linear constraints to problem ($\mathcal{P}_1$):

$$-F_{y,j} \leq F^i_{s,j} \leq F_{y,j}. \tag{16}$$

In the case of a NAND optimization approach, the constraints in Eq. (16) would require dedicated adjoint or direct sensitivity analyses. Instead, due to the SAND approach proposed and discussed in this article, the addition of the constraint of Eq. (16) to problem ($\mathcal{P}_1$) is straightforward. It consists of adding box constraints (i.e. lower and upper bounds) for the optimization variables $F^i_{s,j}$. To impose the constraints of Eq. (16) we follow the continuation approach adopted for imposing the drift constraints (Algorithm (1)). Thus, we consider a sequence of decreasing values for d_{max} and $\mathbf{F}_y$. For each value, we solve problem ($\mathcal{P}_1$), and use the optimal solution found as warm start information for the subsequent optimization analysis. The procedure halts once we find a solution associated with the desired values for $\mathbf{F}_y$, that is, $\bar{\mathbf{F}}_y = [169.0,\ 107.0]$ kN. As a result, we solve a sequence of four sub-problems with decreasing values of d_{max} and $\mathbf{F}_y$, as shown in Table 4.

Sub-problem	1	2	3	4
d_{max} [mm]	15.0	13.0	11.0	9.0
$\mathbf{F}_y$ [kN]	[Inf, Inf]	$1.5\cdot\left[\bar{F}_{y,1}, \bar{F}_{y,2}\right]$	$1.25\cdot\left[\bar{F}_{y,1}, \bar{F}_{y,2}\right]$	$1.0\cdot\left[\bar{F}_{y,1}, \bar{F}_{y,2}\right]$

Table 4: Values of d_{max} and $\mathbf{F}_y$ used in Sec.5.3 for solving problem ($\mathcal{P}_1$) sequentially, as described in Algorithm 1

In this case, the maximum damping coefficient value is set to $c_{d,max} = 10\ \text{kN}\frac{\text{s}}{\text{mm}}$, and we consider the same time discretization of the ground acceleration load as in the preceding case ($\Delta t = 0.004$ s). The resulting problem has the same dimensions as in the previous case. The optimization algorithm converged in 53 s with a total of 146 iterations. The optimized solution consists of damping coefficients $c_{d1} = 6.73\ \text{kN}\frac{\text{s}}{\text{mm}}$ and $c_{d2} = 3.17\ \text{kN}\frac{\text{s}}{\text{mm}}$. The final value of the objective function is $\tau^{opt} = 335.78$ kN. Fig. 14 shows the structural force-displacement plots associated with the

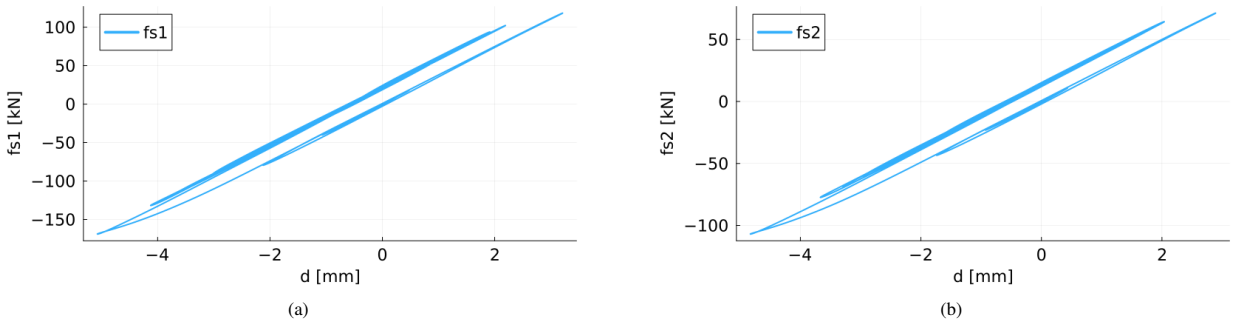

(a) (b)

Figure 14: Optimized structural responses F_{s1} (14a) and F_{s2} (14b) obtained solving problem $\mathcal{P}_1$ while considering 30% of the initial stiffness in the post-yielding phase (i.e. $a = 30\%$ in Eq. (7))

optimized design obtained for the FVDs. Due to the constraints of Eq. (16), the structure exhibits an almost linear elastic behavior. The inelastic deformations are significantly reduced compared to those observed in Fig. 12. Fig. 15, instead, shows the structural force time-history plots associated with the optimized design obtained. The dashed lines mark the yielding limits that are $F_{y,1} = 169.0$ kN and $F_{y,2} = 107.0$ kN. It can be observed that in none of the time steps the structural forces exceed the yielding limit, as expected due to the additional constraints considered for $F^i_{s,j}$.

6. Conclusions

This article presents a novel SAND approach for transient optimization of fluid viscous dampers in seismic retrofitting applications. The purpose of the proposed approach is to optimize the size and placement of both linear and nonlinear fluid viscous dampers for seismic retrofitting of hysteretic structures. The objective function that

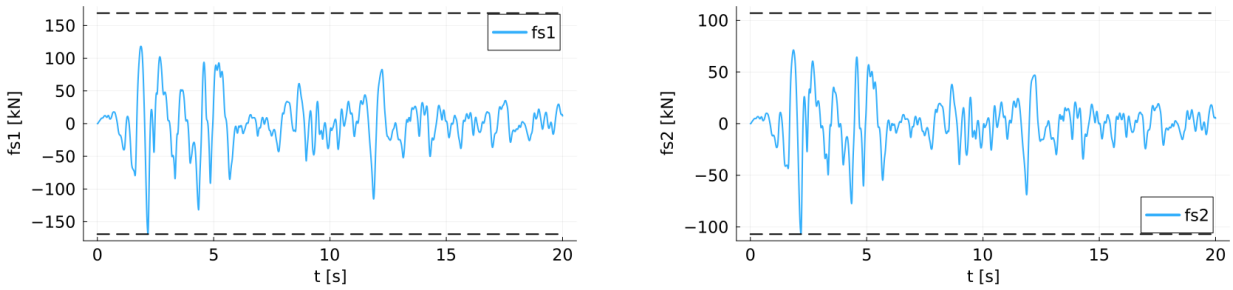

(a) (b)

Figure 15: Optimized structural responses F_{s1} (15a) and F_{s2} (15b) obtained solving problem $\mathcal{P}_1$ with the constraints Eq. (16) while considering 30% of the initial stiffness in the post-yielding phase (i.e. $a = 30\%$ in Eq. (7)). The dashed lines represent the yielding forces' values $F_{y,1} = 169.0$ kN and $F_{y,2} = 107.0$ kN

is minimized is the maximum force in time produced by the viscous dampers. This is equivalent to minimizing the dampers' manufacturing cost. In practice, in fact, the cost of the viscous dampers is proportional to the peak force for which they are designed. With the proposed SAND approach, the structural response quantities are treated as additional variables of the optimization problem. The equations of motion become equality constraints. As a result, during the optimization analysis, there is no need to perform expensive time-history analyses for evaluating the structural response, and adjoint (or direct) sensitivity analyses for calculating the gradients of the functions involved in the problem formulation.

The approach is tested on a 2D hysteretic planar frame in two design scenarios. In the first one, the fluid viscous dampers have a linear behavior. In the second one, the dampers have a nonlinear force-velocity behavior, and the stiffening contribution of the dampers and their supporting braces is also accounted for. We propose and discuss a SAND optimization approach based on the solution of a sequence of sub-problems. Each sub-problem is similar to the original problem but with relaxed upper and lower bounds of the design-driving inter-story drifts constraints. The solution found in each sub-problem is then used in the subsequent sub-problem as warm start information, where the inter-story drift bounds are progressively tightened. The procedure stops once we find an optimal solution that satisfies the desired limits on the inter-story drifts allowed.

The main advantage of the proposed approach lies in its modelling simplicity and flexibility, thanks also to the current state-of-the-art of modern optimization solvers and modelling languages. The proposed approach does not require the development of complex nonlinear time-history analyses and the associated sensitivity analyses for the calculation of the gradients. Thus, in a sense, the development complexity is significantly lower in the case of SAND approaches compared to that of NAND gradient-based approaches. Nevertheless, the reduced development complexity of the proposed approach comes at the cost of computationally more demanding optimization analyses due to the large number of optimization variables. Future studies should focus on: the extension and applicability of the proposed approach to large-scale 3D design cases; the development of efficient strategies for reducing the computational cost of the resulting optimization problems.

Replication of results

The proposed approach, the optimization problems considered, and the structural analysis equations are described in sufficient detail to be implemented. Additionally, all parameters and system matrices used in the numerical experiments are defined in the paper.

Declaration of competing interest

The author confirms that there are no competing interests.

Funding information

This research did not receive any specific grant from funding agencies in the public, commercial, or not-for-profit sectors.

References

S. Akcelyan, D. G. Lignos, T. Hikino, and M. Nakashima. Evaluation of simplified and state-of-the-art analysis procedures for steel frame buildings equipped with supplemental damping devices based on e-defense full-scale shake table tests. *Journal of Structural Engineering*, 142 (6):04016024, 2016.

S. Akcelyan, D. G. Lignos, and T. Hikino. Adaptive numerical method algorithms for nonlinear viscous and bilinear oil damper models subjected to dynamic loading. *Soil Dynamics and Earthquake Engineering*, 113:488–502, 2018.

K. Y. M. Almajhali. Review on passive energy dissipation devices and techniques of installation for high rise building structures. *Structures*, 51: 1019–1029, 2023.

D. Altieri, E. Tubaldi, M. De Angelis, E. Patelli, and A. Dall'Asta. Reliability-based optimal design of nonlinear viscous dampers for the seismic protection of structural systems. *Bulletin of Earthquake Engineering*, 16:963–982, 2018.

J. Arora and Q. Wang. Review of formulations for structural and mechanical system optimization. *Structural and Multidisciplinary Optimization*, 30(4):251–272, 2005.

J. Bezanson, A. Edelman, S. Karpinski, and V. B. Shah. Julia: A fresh approach to numerical computing. *SIAM Review*, 59(1):65–98, 2017.

A. K. Chopra. *Dynamics of Structures. Theory and Applications to Earthquake Engineering*. Prentice Hall, 2012.

P. W. Christensen and A. Klarbring. *An introduction to structural optimization*, volume 153. Springer Science & Business Media, 2008.

M. Constantinou and M. Symans. Experimental study of seismic response of buildings with supplemental fluid dampers. *The Structural Design of Tall Buildings*, 2(2):93–132, 1993.

M. C. Constantinou and M. Symans. *Experimental and analytical investigation of seismic response of structures with supplemental fluid viscous dampers*. National Center for Earthquake Engineering Research Buffalo, NY, 1992.

G. Dargush and R. Sant. Evolutionary aseismic design and retrofit of structures with passive energy dissipation. *Earthquake engineering & structural dynamics*, 34(13):1601–1626, 2005.

D. De Domenico and G. Ricciardi. Improved stochastic linearization technique for structures with nonlinear viscous dampers. *Soil Dynamics and Earthquake Engineering*, 113:415–419, 2018.

D. De Domenico, G. Ricciardi, and I. Takewaki. Design strategies of viscous dampers for seismic protection of building structures: a review. *Soil dynamics and earthquake engineering*, 118:144–165, 2019.

A. Filiatrault and C. Christopoulos. *Principles of passive supplemental damping and seismic isolation*. IUSS Press, Pavia, Italy, 2006.

FIP MEC. FIP MEC S.r.l. `https://www.fipmec.it/`.

I. Gidaris and A. A. Taflanidis. Performance assessment and optimization of fluid viscous dampers through life-cycle cost criteria and comparison to alternative design approaches. *Bulletin of Earthquake Engineering*, 13:1003–1028, 2015.

R. T. Haftka. Simultaneous analysis and design. *AIAA Journal*, 23:1099–1103, 1985. ISSN 00011452. doi: 10.2514/3.9043.

O. Idels and O. Lavan. Optimization-based seismic design of steel moment-resisting frames with nonlinear viscous dampers. *Structural Control and Health Monitoring*, 28(1):e2655, 2021a.

O. Idels and O. Lavan. Performance-based seismic retrofitting of frame structures using negative stiffness devices and fluid viscous dampers via optimization. *Earthquake Engineering & Structural Dynamics*, 50(12):3116–3137, 2021b.

S. Infanti, H. Kang, and M. Castellano. Retrofit of bridges in korea using viscous damper technology. In *Proceedings of the 13th World Conference on Earthquake Engineering, Vancouver BC*, page 2211, 2004.

J. Iori. Design optimization of a wind turbine blade under non-linear transient loads using analytic gradients. In *Journal of Physics: Conference Series*, volume 1618, page 042032. IOP Publishing, 2020.

X. Ji, T. Hikino, K. Kasai, and M. Nakashima. Damping identification of a full-scale passively controlled five-story steel building structure. *Earthquake engineering & structural dynamics*, 42(2):277–295, 2013.

JuMP community. Ipopt.jl. `https://github.com/jump-dev/Ipopt.jl`, 2023.

T. Larsson and M. R. . Snnqvist. Simultaneous structural analysis augmented lagrangian duality, 1995.

O. Lavan and O. Amir. Simultaneous topology and sizing optimization of viscous dampers in seismic retrofitting of 3d irregular frame structures. *Earthquake engineering & structural dynamics*, 43(9):1325–1342, 2014.

O. Lavan and R. Levy. Optimal design of supplemental viscous dampers for irregular shear-frames in the presence of yielding. *Earthquake engineering & structural dynamics*, 34(8):889–907, 2005.

O. Lavan and R. Levy. Optimal peripheral drift control of 3D irregular framed structures using supplemental viscous dampers. *Journal of Earthquake Engineering*, 10(06):903–923, 2006a.

O. Lavan and R. Levy. Optimal design of supplemental viscous dampers for linear framed structures. *Earthquake engineering & structural dynamics*, 35(3):337–356, 2006b.

R. Levy and O. Lavan. Fully stressed design of passive controllers in framed structures for seismic loadings. *Structural and Multidisciplinary Optimization*, 32(6):485–498, 2006.

D. Lopez Garcia and T. Soong. Efficiency of a simple approach to damper allocation in mdof structures. *Journal of structural control*, 9(1):19–30, 2002.

M. Lubin, O. Dowson, J. D. Garcia, J. Huchette, B. Legat, and J. P. Vielma. Jump 1.0: Recent improvements to a modeling language for mathematical optimization. *Mathematical Programming Computation*, 2023. In press.

R. J. McNamara and D. P. Taylor. Fluid viscous dampers for high-rise buildings. *The structural design of tall and special buildings*, 12(2):145–154, 2003.

C. E. Orozco and O. N. Ghattas. Sparse approach to simultaneous analysis and design of geometrically nonlinear structures. *AIAA Journal*, 30: 1877–1885, 1992. ISSN 00011452. doi: 10.2514/3.11150.

C. E. Orozco and O. N. Ghattas. A reduced sand method for optimal design of non-linear structures. *International Journal for Numerical Methods in Engineering*, 40(15):2759–2774, 1997.

E. Parcianello, C. Chisari, and C. Amadio. Optimal design of nonlinear viscous dampers for frame structures. *Soil Dynamics and Earthquake Engineering*, 100:257–260, 2017.

N. Pollini. Fail-safe optimization of viscous dampers for seismic retrofitting. *Earthquake Engineering & Structural Dynamics*, 49(15):1599–1618, 2020.

N. Pollini. On simultaneous analysis and design optimization for seismic retrofitting with fluid viscous dampers. *Structural and Multidisciplinary Optimization*, 2023.

N. Pollini, O. Lavan, and O. Amir. Towards realistic minimum-cost optimization of viscous fluid dampers for seismic retrofitting. *Bulletin of Earthquake Engineering*, 14:971–998, 2016.

N. Pollini, O. Lavan, and O. Amir. Minimum-cost optimization of nonlinear fluid viscous dampers and their supporting members for seismic retrofitting. *Earthquake Engineering & Structural Dynamics*, 46(12):1941–1961, 2017.

N. Pollini, O. Lavan, and O. Amir. Adjoint sensitivity analysis and optimization of hysteretic dynamic systems with nonlinear viscous dampers. *Structural and Multidisciplinary Optimization*, 57(6):2273–2289, 2018a.

N. Pollini, O. Lavan, and O. Amir. Optimization-based minimum-cost seismic retrofitting of hysteretic frames with nonlinear fluid viscous dampers. *Earthquake Engineering & Structural Dynamics*, 47(15):2985–3005, 2018b.

U. T. Ringertz. An algorithm for optimization of non-linear shell structures. *International Journal for Numerical Methods in Engineering*, 38: 299–314, 1995. ISSN 10970207. doi: 10.1002/nme.1620380209.

L. A. Schmit and R. L. Fox. An integrated approach to structural synthesis and analysis. *AIAA Journal*, 3(6):1104–1112, 1965.

H. Shin and M. Singh. Minimum failure cost-based energy dissipation system designs for buildings in three seismic regions–part i: Elements of failure cost analysis. *Engineering structures*, 74:266–274, 2014a.

H. Shin and M. Singh. Minimum failure cost-based energy dissipation system designs for buildings in three seismic regions–part ii: Application to viscous dampers. *Engineering Structures*, 74:275–282, 2014b.

M. V. Sivaselvan and A. M. Reinhorn. Hysteretic models for deteriorating inelastic structures. *Journal of engineering mechanics*, 126(6):633–640, 2000.

P. G. Somerville. *Development of ground motion time histories for phase 2 of the FEMA/SAC steel project*. SAC Joint Venture, 1997.

T. T. Soong and G. F. Dargush. Passive energy dissipation systems in structural engineering, john wiley & sons. *New York*, page 282, 1997.

M. Stolpe and K. Svanberg. A note on stress-constrained truss topology optimization. *Structural and multidisciplinary optimization*, 25(1):62–64, 2003.

I. Takewaki. Optimal damper placement for planar building frames using transfer functions. *Structural and Multidisciplinary Optimization*, 20: 280–287, 2000.

D. P. Taylor. History, design, and applications of fluid dampers in structural engineering. In *Passive Structural Control Symposium*, pages 13–14, 2002.

Taylor Devices. Taylor Devices, Inc. `https://www.taylordevices.com/`.

The Julia Project. Julia Programming Language. `https://julialang.org/`, 2023.

E. Tubaldi, M. Barbato, and A. Dall'Asta. Performance-based seismic risk assessment for buildings equipped with linear and nonlinear viscous dampers. *Engineering Structures*, 78:90–99, 2014.

E. Tubaldi, L. Ragni, and A. Dall'Asta. Probabilistic seismic response assessment of linear systems equipped with nonlinear viscous dampers. *Earthquake Engineering & Structural Dynamics*, 44(1):101–120, 2015.

A. Wächter and L. T. Biegler. On the implementation of an interior-point filter line-search algorithm for large-scale nonlinear programming. *Mathematical programming*, 106:25–57, 2006.

Q. Wang and J. S. Arora. Alternative formulations for transient dynamic response optimization. *AIAA journal*, 43(10):2188–2195, 2005.

Q. Wang and J. S. Arora. Several simultaneous formulations for transient dynamic response optimization: An evaluation. *International journal for numerical methods in engineering*, 80(5):631–650, 2009.

C. Wu and J. Arora. Simultaneous analysis and design optimization of nonlinear response. *Engineering with Computers*, 2(1):53–63, 1987.

R.-H. Zhang and T. Soong. Seismic design of viscoelastic dampers for structural applications. *Journal of structural engineering*, 118(5):1375–1392, 1992.